Deadbeat Predictive Current Control for High-Speed PMSM Drives with Low Switching-to-Fundamental Frequency Ratios

Shangjian Dai, Jiabin Wang, *Senior Member, IEEE*, Zhigang Sun, and Ellis Chong

Abstract—This paper analyzes the conventional dq-frame model-based deadbeat predictive current control (DBPCC) methods for high-speed permanent magnet synchronous machine (PMSM) drives with low switching–to–fundamental frequency ratios (SFRs). It shows that the state-of-the-art compensation schemes of control delay and rotor movement effect can improve the control performance but the problem still arises at very high speeds with very low SFRs. Therefore, this paper presents a novel DBPCC method for high-speed PMSM drives. The proposed method tracks the machine stator flux vector in the stationary frame to achieve deadbeat control of the dq-axis currents. The control delay and rotor movement effect are both precisely considered. Consequently, the control performance and stability of the proposed DBPCC can be guaranteed at high speeds. Extensive simulations and experiments have been performed on a prototype high-speed PMSM drive. The effectiveness of the proposed method and its superiorities against the field-oriented control (FOC) and the conventional DBPCCs have all been demonstrated.

Index Terms— Deadbeat predictive current control, high-speed permanent magnet synchronous machine, low switching-to-fundamental frequency ratio, flux tracking.

I. INTRODUCTION

Due to high efficiency and high power density, high-speed permanent magnet synchronous machine (PMSM) drives have currently been widely researched for many applications, including electric vehicles [1], more electric aircrafts [2], [3], high-speed spindles, and compressors, etc [4]. The high-speed drive usually features high fundamental frequencies, e.g. 2 kHz for a starter/generator of aircrafts [2], [3]. Given the switching frequency limit of semiconductor devices, such as 10~20 kHz typically for IGBTs, the high-speed PMSM drive can exhibit very low switching-to-fundamental frequency ratios (SFRs).

Fig. 1 shows the typical timing sequence of a digital controller [5], where at each step the phase currents are sampled and the stator voltage reference for the next step are synthesized. With the superior dynamic response and higher voltage utilization, space vector modulation (SVM) is usually employed. The sampling/control period, T_s is usually set as the same as or half of the switching period. Hence, the low SFRs will also lead to low sampling-to-fundamental frequency ratios. As can be seen, the control delay consists of both the one-step processing (i.e. sampling and calculation) delay and the PWM delay since the stator voltage or PWM signals can only be updated at the beginning of each step and take one step to complete. For high-speed PMSMs with low SFRs, the control delay can be very large. As a result, it would significantly deteriorate the dynamic response and may cause oscillation and even instability of the drive system [5]–[7]. Thus, the investigation on robust and high bandwidth control of high-speed PMSM drives with low SFRs are of great importance.
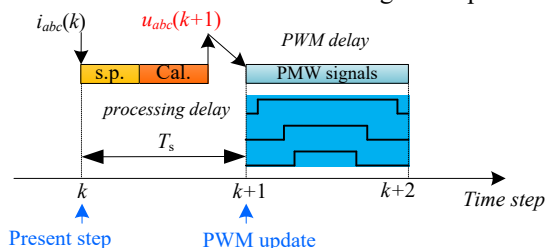
Fig. 1 Typical timing sequence diagram of a digital motor controller.

Extensive researches have been reported to improve the classic field-oriented control (FOC) for high-speed PMSM drives with low SFRs [5]–[8]. The control delay can be simply modelled as a first-order system with the time constant of $1.5T_s$ and compensated accordingly based on the complex vector transfer function [8]. However, the majority of the researches to address this problem are based on the more accurate zero-order holder inverter model [5]–[7], in which the inverter output voltage in the stationary frame is assumed constant over a time-step. Based on this inverter model, the control delay is effectively caused by the rotor movement during the control period [5]. The resultant phase delay and the magnitude distortion of stator voltage vector can be analytically derived and compensated. This delay compensation method can effectively extend the operating speed range and enhance the control performance of PMSM at high speeds [5]. However, as reported in [6], when the SFR is less than 10, the high-speed drive could lose stability even with the delay compensation and

accurate machine parameters. A solution which employs the complex vector current regulator with one-step prediction for active damping was proposed in [6] to stabilize the FOC at very low SFRs. However, the current dynamic response was compromised and the cause of the stability problem with SFR less than 10 was not clearly understood. A discrete current regulator synthesized based on the z-domain machine model was proposed in [7]. It has been shown by the z-domain analysis that the current control with the directly synthesized discrete current regulator is best among various current regulator designs under the FOC and can give stable control at very low SFRs. However, this method is not experimentally evaluated for SFR<12. Moreover, although stable control can be achieved by the appropriate design of the FOC current controller, the available control bandwidth will decrease as the SFR reduces.

Therefore, the control techniques with the well-known advantage of fast dynamic response, such as direct torque control [9], finite-control-set model predictive control (FCS-MPC) [10], and deadbeat control [11], [12], [21], [13]–[20] are more attractive for high-speed PMSM drives with low SFRs. Among these methods, the deadbeat control is more superior since it incorporates SVM and can contribute to both fast dynamic response and low current harmonics with constant switching frequency. The deadbeat control can be further divided to two groups, i.e. deadbeat predictive current control (DBPCC) [12]–[21] and deadbeat direct flux and torque control (DB-DTFC) [11]. Compared to DB-DTFC, DBPCC does not require complicated flux and torque observer and the calculation of the reference voltage vector is simpler. Hence, DBPCC is regarded more attractive for high bandwidth control of high-speed PMSM drives [17], [18] and thereby further investigated in this paper.

The DBPCC is usually based on the discretized machine model in the dq frame and constitutes two steps [12]–[18], i.e., the one-step current prediction and the calculation of the stator voltage to realize deadbeat control. By one-step current prediction, the one-step processing delay can be well compensated with the accurate machine model. Moreover, extensive studies have been carried out to increase the parameter robustness of DBPCC [15]–[17]. However, the rotor movement effect, which causes the so-called PWM delay in FOC [5], is usually neglected in the literatures on DBPCC. It will cause the similar problem in DBPCC because of the rotor-position dependent conversion of the reference voltage from the rotational frame to the stationary frame. Only a few literature [18] for high-speed PMSM drives pays attention to this problem and compensates the rotor movement based on the zero-holder inverter model, same as that for FOC [5]. However, as will be analyzed and demonstrated in this paper, this kind of compensation is not sufficient for DBPCC at high speeds with very low SFRs.

Instead of using the dq-frame based machine model, the stationary frame-based voltage model of PMSMs can be employed for DBPCC, so that the synthesized reference voltage vector is in the stationary frame and its implementation by SVM will not be affected by the rotor movement. However, the rotor movement and one-step processing delay effects on the current and reference voltage predictions have not been precisely considered in the existing literature. In [19], the stationary

frame based model is employed, but the rotor movement influence on the back EMF is neglected. As presented in [20], the large rotor movement in high speed can still cause a large prediction error in current using the stationary frame-based voltage model of PMSMs by linear current approximation. In [21], a stator flux controller is employed to control the phase current of high-speed PMSM. It is not affected by the rotor movement, however, it requires the look-up-table (LUT) between phase current magnitude and phase flux. Moreover, it does not generally apply to current vector control with any combination of d- and q-axis currents and one-step current prediction is not included.

With the emerging wide band gap (WBG) semiconductor devices technology [22], higher switching frequency can be employed. While this can circumvent some problems of the conventional control methods at a high speed by increasing the operating SFRs, the high dv/dt and high switching frequency of WBG devices may lead to many undesired problems, such as intensified parasitic influences and oscillations, increased electromagnetic interference (EMI), accelerated insulation degradation, etc. Besides, in general, the control challenge with low SFRs still exists at higher speeds for an optimal solution when the fundamental frequency further increases.

Based on the foregoing literature review, this paper will focus on the analysis of rotor movement influence on the conventional dq-frame based DBPCCs and develop a novel DBPCC for high-speed PMSM drives with low SFRs. The main contributions of this paper can be summarized as follows.

1) To the best of the authors' knowledge, this paper demonstrates for the first time the problem of the dq-frame based DBPCCs at high speeds and suggests their appropriate applicable SFR ranges, accordingly.

2) A novel DBPCC based on the stator flux vector tracking in the stationary frame is proposed, in which the processing delay and the rotor movement effects in high-speed PMSM drives are both precisely taken into accounts. The control performance of the proposed method is hardly affected by the high operating speeds of PMSM. It can realize excellent deadbeat control of dq-axis currents in two time-steps and without cross-coupling in the whole speed and SFR ranges.

II. CONVENTIONAL DBPCCs AND ROTOR MOVEMENT COMPENSATION

For notational convenience, the complex vector representation of PMSM models is employed in this paper [23]. In the complex vector models, the current, voltage, flux vectors in the dq-frame/αβ-frame are expressed by complex numbers, with the d-axis/α-axis as the real axis and q-axis/β-axis as the imaginary axis, e.g. the dq-axis current vector is expressed as $\boldsymbol{i}_{dq} = i_d + j \cdot i_q$, where j is the imaginary operator, i_d and i_q are the d-axis current and q-axis current, respectively.

Ignoring space and time harmonics, the PMSM model in the dq frame is given by

$$\boldsymbol{u}_{dq} = L_s \frac{d\boldsymbol{i}_{dq}}{dt} + R\boldsymbol{i}_{dq} + j\omega_e \left(L_s \boldsymbol{i}_{dq} + \psi_m \right) \tag{1}$$

where, $\boldsymbol{u}$ and $\boldsymbol{i}$ denote the stator voltage and current vectors, respectively; the subscript, dq denotes the variable in the dq

frame; L_s is the synchronous inductance; R is the phase resistance; ω_e is the electric angular speed and ψ_m is the PM flux linkage. For interior mounted PMSMs (IPMSMs), the d-axis inductance, L_d, and q-axis inductance, L_q, should be employed for the corresponding axes, respectively.

By forward Euler approximation, the discrete model of PMSM can be obtained as (2), where T_s is the sampling/control period, (k) denotes the quantities at step k. In this paper, to investigate the worst-case scenario, T_s is set equal to the switching period.

$$\boldsymbol{u}_{dq}(k) = L_s \frac{\boldsymbol{i}_{dq}(k+1) - \boldsymbol{i}_{dq}(k)}{T_s} + R\boldsymbol{i}_{dq}(k) + j\omega_e\big(L_s\boldsymbol{i}_{dq}(k) + \psi_m\big) \tag{2}$$

A. Conventional DBPCC without rotor movement compensation

The DBPCC incorporates two procedures, namely, predicting the next step currents and synthesizing the reference voltage vector in the subsequent step to achieve dead-beat control of the reference currents.

According to (2), the dq-axis currents at the next sampling instant, $\hat{\boldsymbol{i}}_{dq}(k+1)$ can be predicted by

$$\hat{\boldsymbol{i}}_{dq}(k+1) = \frac{T_s}{L_s}\big[\boldsymbol{u}_{dq}(k) - R\boldsymbol{i}_{dq}(k) - j\omega_e\big(L_s\boldsymbol{i}_{dq}(k) + \psi_m\big)\big] + \boldsymbol{i}_{dq}(k) \tag{3}$$

where the actual dq-axis voltage vector, $\boldsymbol{u}_{dq}(k)$ is usually assumed equal to the reference, $\boldsymbol{u}_{dq}^*(k)$, synthesized at the previous step; the cap, ^, denotes the estimated value and the superscript, *, denotes the reference value.

With the predicted currents, $\hat{\boldsymbol{i}}_{dq}(k+1)$ and the given reference currents, $\boldsymbol{i}_{dq}^*$, the reference dq-axis voltages in step $k+1$, i.e. $\boldsymbol{u}_{dq}^*(k+1)$ can be synthesized as

$$\boldsymbol{u}_{dq}^*(k+1) = L_s \cdot \frac{\boldsymbol{i}_{dq}^* - \hat{\boldsymbol{i}}_{dq}(k+1)}{T_s} + R\hat{\boldsymbol{i}}_{dq}(k+1) + j\omega_e\big(L_s\hat{\boldsymbol{i}}_{dq}(k+1) + \psi_m\big) \tag{4}$$

Assume that the speed is constant during the control steps, the reference $\alpha\beta$-axis voltages, $\boldsymbol{u}_{\alpha\beta}(k+1)^*$ can be derived as

$$\boldsymbol{u}_{\alpha\beta}(k+1)^* = \boldsymbol{u}_{dq}(k+1)^* \cdot e^{j(\theta_e(k)+\omega_e T_s)} \tag{5}$$

where, the subscript, $\alpha\beta$ denotes the variable in the $\alpha\beta$ frame; θ_e is electrical angular position of the rotor; e is the base of the natural logarithmic function and e^{jx} represents the anti-clockwise rotation of a vector by x radian.

With SVM, the synthesized reference voltage vector in (5) can then be implemented by the inverter.

As can be seen, by the one-step current prediction in (3) and the coordinate transformation in (5), the one-step processing delay of the digital control is compensated. However, the rotor movement during the PWM implementation process are not accounted. Hence, in this paper, the DBPCC based on (3)~(5) is referred to as conventional DBPCC without rotor movement compensation.

B. Conventional DBPCC with rotor movement compensation

To compensate the rotor movement effect, the zero-order holder inverter model is usually employed in the literatures [5],

[18]. It is assumed that the instantaneous stator voltages equal to the reference stator voltages in the stationary frame. This assumption implies that the reference $\alpha\beta$-axis voltage is rotating at the same rotor speed but in the opposite direction viewed from the rotor. Hence, in order to have the same volt-second or the average voltage in the dq frame as the reference dq-axis voltages given in (4) for the deadbeat control, the coordinate transformation, (5), should be modified [5] as

$$\boldsymbol{u}_{\alpha\beta}(k+1)^* = \frac{1}{K(\omega_e T_s)}\boldsymbol{u}_{dq}(k+1)^* \cdot e^{j(\theta_e(k)+\omega_e T_s)} \tag{6}$$

$$K(\omega_e T_s) = \frac{2\sin(\omega_e T_s/2)}{\omega_e T_s} \cdot e^{-j\omega_e T_s/2} \tag{7}$$

Fig. 2 shows the unified block diagram of the conventional DBPCCs. As seen, both the conventional DBPCCs consider the one-step processing delay. For the conventional DBPCC without rotor movement compensation, $K(\omega_e T_s)$ is set to 1 while calculated by (7) with rotor movement compensation.
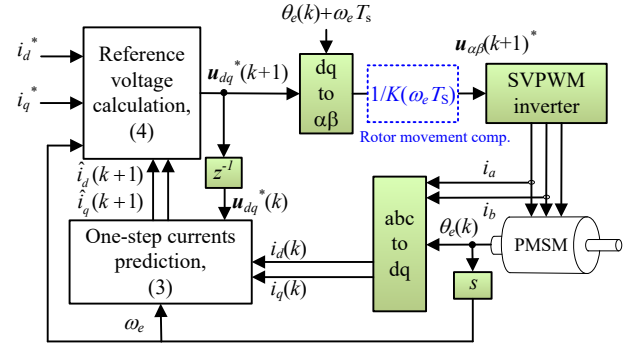

Fig. 2 A unified block diagram of the conventional DBPCCs without rotor movement compensation ($K(\omega_e T_s) = 1$) and with rotor movement compensation ($K(\omega_e T_s)$ is calculated by (7)).

III. ANALYSIS OF CONVENTIONAL DBPCCs AT HIGH SPEEDS

Ignoring the resistive voltage drops, the reference $\alpha\beta$-axis voltage vector can be realized correctly by an ideal inverter with SVM. The corresponding stator flux increment in the $\alpha\beta$ frame, namely, the voltage-second input, $\boldsymbol{VS}_{\alpha\beta}(k)$, applied to a motor during the kth step is given by

$$\boldsymbol{VS}_{\alpha\beta}(k) = \int_0^{T_s} \boldsymbol{u}_{\alpha\beta}(t_k + t)dt = T_s\boldsymbol{u}_{\alpha\beta}(k)^* \tag{8}$$

where $\boldsymbol{u}_{\alpha\beta}(t_k + t)$ denotes the actual instantaneous stator voltage vector at the time instant of $t_k + t$, t_k is the time instant at the beginning of the kth step, and $\boldsymbol{u}_{\alpha\beta}(k)^*$ is the reference stator voltage vector at the kth step in the $\alpha\beta$ frame.

From (8), the volt-second input to the motor expressed in the dq frame can be derived as

$$\boldsymbol{VS}_{dq}(k) = e^{-j\theta_e(k)}\int_0^{T_s} \boldsymbol{u}_{\alpha\beta}(t_k + t) \cdot e^{-j\omega_e t}dt \tag{9}$$

Therefore, the actual average voltage in the dq frame can be derived as

$$\boldsymbol{u}_{dq\_av}(k) = \frac{e^{-j\theta_e(k)}}{T_s}\int_0^{T_s} \boldsymbol{u}_{\alpha\beta}(t_k + t) \cdot e^{-j\omega_e t}dt \tag{10}$$

Further, with the reference dq-axis voltage in the kth step, $\boldsymbol{u}_{dq}(k)^*$, the average realization error of the reference dq-axis voltage in step k can be expressed as

$$err_{udq}(k) = \frac{e^{-j\theta_e(k)}}{T_s}\int_0^{T_s}\boldsymbol{u}_{\alpha\beta}(t_k+t)\cdot e^{-j\omega_e t}dt - \boldsymbol{u}_{dq}(k)^* \tag{11}$$

By substituting (5) and (6) associated with step k into (11), the average dq-axis voltage errors can be obtained for the conventional DBPCCs without and with rotor movement compensation in (12) and (13), respectively.

$$err_{udq1}(k) = \left[\boldsymbol{u}_{\alpha\beta}(k)^* - \frac{1}{T_s}\int_0^{T_s}\boldsymbol{u}_{\alpha\beta}(t_k+t)\cdot e^{-j\omega_e t}dt\right]\cdot e^{-j\theta_e(k)} \tag{12}$$

$$err_{udq2}(k) = \frac{e^{-j\theta_e(k)}}{T_s}\int_0^{T_s}\left[\boldsymbol{u}_{\alpha\beta}(t_k+t) - \boldsymbol{u}_{\alpha\beta}(k)^*\right]\cdot e^{-j\omega_e t}dt \tag{13}$$

As can been seen in (12), without rotor movement compensation, zero voltage error can only be achieved when the speed is low, i.e., $e^{-j\omega_e t}$ is close to 1.

From (13), with rotor movement compensation, if the assumption that the instantaneous stator voltage vector in the stationary frame equals to the reference one is true, zero voltage error can be guaranteed regardless of speed. However, as the SFR reduces greatly at high speeds, i.e. the rotor movement in a time-step, equal to $2\pi/$SFR, increases to very large value, the instantaneous voltage, $\boldsymbol{u}_{\alpha\beta}(t_k+t)$, may differ significantly from $\boldsymbol{u}_{\alpha\beta}(k)^*$ in (13), of which the integration over the time-step is not zero and can increase as the voltage vector magnitude increases at high speeds. Consequently, although the rotor movement compensation scheme is employed, the large voltage error will still occur at high speeds due to relatively large rotor movement.

In high-speed PMSMs, their synchronous inductances are usually low because the number of series connected turns in a phase winding is low. Consequently small average voltage errors expressed in (12) and (13) would finally lead to high current control errors, deteriorating both the transient and steady-state control performances.
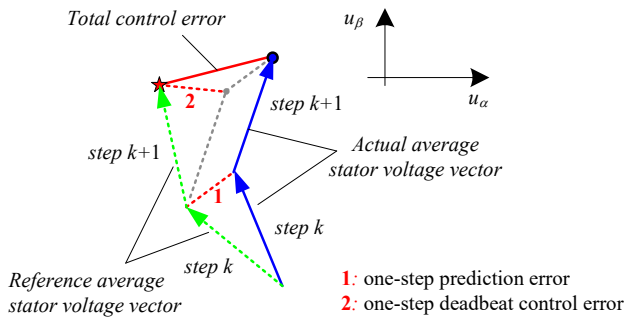

Fig. 3 Illustration of the total control error due to the average voltage error in (12) and (13).

Additionally, the average voltage error will also affect the accuracy of the one-step prediction in (3) since the reference dq-axis voltage vector used in prediction will also be different from the actual one. As illustrated in Fig. 3, the difference between the synthesized reference average voltage and the

actual one will contribute to both one-step prediction error and one-step deadbeat control error, which constitute the total control error. Thus, the rotor movement over the two time-steps rather than only a time-step will influence the control performance of DBPCC and it can be very large at high speeds.

TABLE I
PARAMETERS OF THE PROTOTYPE HIGH-SPEED PMSM DRIVE

Parameter	Magnitude
Number of poles pairs	2
Phase resistance	20 mΩ
d-axis inductance	125 μH
q-axis inductance	134.2 μH
PM flux linkage	9.83 mWb
Rated phase current (peak)	50 A
Rated torque	1.5 Nm
Rated speed	30,000 rpm
Rated power	5 kW
DC-link voltage	270 V
Switching/Sampling frequency	10 kHz
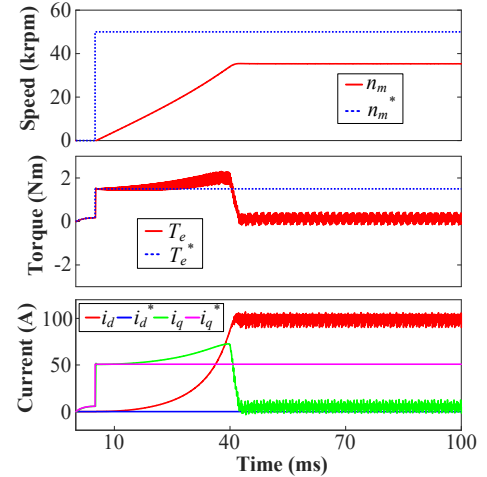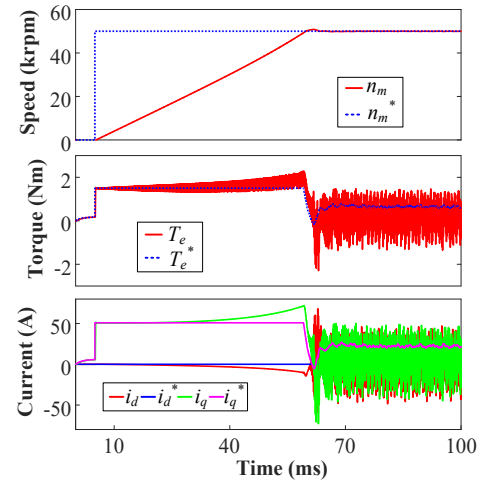
Fig. 4 Speed, torque and sampled dq axis current waveforms of the prototype high-speed PMSM drives accelerating form standstill to 50,000 rpm with 10% rated load torque and the speed control bandwidth of 50 Hz, using the conventional DBPCC (a) without compensation (b) with compensation.

It is worth mentioning that the resultant current errors in steady states could potentially be compensated in a disturbance-

observer based DBPCC [15]–[17]. However, in transients with deadbeat control, since the disturbance caused by the average voltage error can be significant, the transient performance degradation cannot be dealt with easily for the drive with low SFRs even if the structure of the disturbance observer is very complex [24].

By way of example, the simulation results in Fig. 4 demonstrate the problems caused by the aforementioned average voltage errors of the conventional DBPCCs at high speeds, where the high-speed machine is accelerated from 0 to 50,000 rpm (SFR=6). The parameters of the prototype machine drive are given in Table I and the detailed simulation conditions are introduced in Section V. As can be seen from the waveforms, as the machine speed increases, large control errors will occur in both the dq-axis currents. Without rotor movement compensation, the conventional DBPCC cannot achieve the reference speed since the large positive d-axis current has caused voltage saturation. With rotor movement compensation, the control performance improves but the current errors are very significant at higher speeds where large current ripples and oscillations can be seen when the speed reaches the steady state.

IV. PROPOSED DBPCC

A novel DBPCC robust to the large rotor movement at high speeds is proposed in this section. The proposed DBPCC also consists two steps, i.e. one-step prediction of stator flux and current, and reference voltage synthesis of deadbeat control. However, these two steps are fundamentally based on the machine model in the stationary frame, i.e.

$$\boldsymbol{\psi}_{\alpha\beta} = \int (\boldsymbol{u}_{\alpha\beta} - R\boldsymbol{i}_{\alpha\beta})dt \qquad (14)$$

where $\boldsymbol{\psi}$ denotes the stator flux vector.

A. One-step prediction of stator flux and current

Neglecting the inverter nonlinearity, the integration of stator voltage over time can be assumed as the product of the reference stator voltage and time-step. Hence, using forward Euler approximation, (14) can be discretized as

$$\boldsymbol{\psi}_{\alpha\beta}(k+1) = \boldsymbol{\psi}_{\alpha\beta}(k) + T_s\boldsymbol{u}_{\alpha\beta}(k)^* - RT_s\boldsymbol{i}_{\alpha\beta}(k) \qquad (15)$$

It should be noted that, according to the principle of SVM, (15) gives an accurate estimation of the voltage integration component in (14) and is independent of the rotor movement. The discretization error is only determined by the estimation error on the resistive voltage drop, i.e. $\int R\boldsymbol{i}_{\alpha\beta}dt - RT_s\boldsymbol{i}_{\alpha\beta}(k)$. It is negligible at high speeds and can be reduced effectively using the trapezoidal approximation when the resistive voltage drop needs to be accounted.

Considering the current-flux model of PMSMs,

$$\boldsymbol{\psi}_{dq} = L_s\boldsymbol{i}_{dq} + \psi_m \qquad (16)$$

the stator fluxes at step k in the synchronous and stationary frames can be obtained respectively as

$$\boldsymbol{\psi}_{dq}(k) = L_s\boldsymbol{i}_{dq}(k) + \psi_m \qquad (17)$$

$$\boldsymbol{\psi}_{\alpha\beta}(k) = [L_s\boldsymbol{i}_{dq}(k) + \psi_m] \cdot e^{j\theta_e(k)} \qquad (18)$$

Substituting (18) into (15) gives the predicted stator flux at step $k+1$,

$$\begin{aligned}\boldsymbol{\psi}_{\alpha\beta}(k+1) = &[L_s\boldsymbol{i}_{dq}(k) + \psi_m] \cdot e^{j\theta_e(k)} \\ &+ T_s\boldsymbol{u}_{\alpha\beta}(k)^* - RT_s\boldsymbol{i}_{\alpha\beta}(k)\end{aligned} \qquad (19)$$

The motor speed can be regarded as constant due to the relative large mechanical time constant compared to the control time-step, thus the rotor position at step $k+1$ can be readily calculated as $\theta_e(k) + \omega_e T_s$.

Again, considering the inverse of the current-flux model of PMSMs,

$$\boldsymbol{i}_{dq} = \frac{\boldsymbol{\psi}_{dq} - \psi_m}{L_s} \qquad (20)$$

the dq-axis currents at step $k+1$ can be obtained from (20) as

$$\boldsymbol{i}_{dq}(k+1) = \frac{\boldsymbol{\psi}_{\alpha\beta}(k+1) \cdot e^{-j[\theta_e(k)+\omega_e T_s]} - \psi_m}{L_s} \qquad (21)$$

With (19) and (21), the one-step prediction of stator flux and current can be achieved. It can be found that the coordinate system transformation of the reference stator voltages is avoided and the rotor movement is explicitly taken into account solely based on the assumption of constant rotor speed. Hence, the one-step prediction is independent of the rotor movement during the PWM implementation process.

It is worth noting that for the PMSMs with large nonlinearity, such as IPMSMs, the linear current-flux model of (17) and inverse current-flux model of (20) should be replaced by the nonlinear ones, e.g. the high-fidelity PMSM mode [25] based on LUTs of calibrated finite element analysis (FEA) results. Nevertheless, for high-speed surface-mounted PMSM (SPMSMs), the machine is usually linear across the operation range due to the relatively large effective air gap [1]–[3]. Hence, for simplicity, the linear current model with the measured inductances and PM flux linkage is used in this paper and proves sufficient in the later experiment results.

B. Reference voltage synthesis of deadbeat control

Assume that the current demands maintain unchanged over the time-steps, i.e. $\boldsymbol{i}_{dq}(k)^* = \boldsymbol{i}_{dq}(k+2)^*$, the reference stator flux in the stationary frame at step $k+2$ is given by

$$\boldsymbol{\psi}_{\alpha\beta}(k+2)^* = [L_s\boldsymbol{i}_{dq}(k)^* + \psi_m] \cdot e^{j[\theta_e(k)+2\omega_e T_s]} \qquad (22)$$

Referring back to the stationary frame model in (14) and its discretization of (15), the reference stator voltage in the stationary frame can be computed as

$$\begin{aligned}\boldsymbol{u}_{\alpha\beta}(k+1)^* = &\frac{\boldsymbol{\psi}_{\alpha\beta}(k+2)^* - \boldsymbol{\psi}_{\alpha\beta}(k+1)}{T_s} \\ &+ R\boldsymbol{i}_{dq}(k+1) \cdot e^{j[\theta_e(k)+\omega_e T_s]}\end{aligned} \qquad (23)$$

where $\boldsymbol{i}_{dq}(k+1)$, $\boldsymbol{\psi}_{\alpha\beta}(k+1)$ and $\boldsymbol{\psi}_{\alpha\beta}(k+2)^*$ are provided in (21), (19) and (22), respectively.

As can be seen from (23), the reference stator voltage to achieve deadbeat control is obtained directly based on stationary frame. It can be implemented by SVM accurately and requires no coordinate conversion. Hence, the voltage errors in (12) and (13) associated with the conventional DBPCC methods are avoided. The control performance of the proposed method will not be affected by the large rotor movement at high speeds.

C. Implementation

Fig. 5 shows the block diagram of the proposed DBPCC, where the inputs are the reference dq-axis current demands and the outputs are the reference stator voltages in the stationary frame. To maximize the voltage utilization, hexagon boundary of voltage is used rather than the inscribed circle limit. For simplicity and good performance, the minimum phase error scheme is employed i.e. when the reference voltage vector is outside the boundary, its phase angle is kept unchanged while the length is shortened to the hexagon boundary.

Fig. 6 illustrates the high-speed SPMSM drive system with the speed control as the outer loop and the proposed DBPCC as the inner current control loop. The q-axis current reference is derived from the speed PI regulator and the d-axis reference is set to 0, however for general application if the flux weakening operation is required, the flux weakening schemes based on the feedforward or/and feedback methods [26] can be easily integrated in by changing the d-axis reference accordingly.
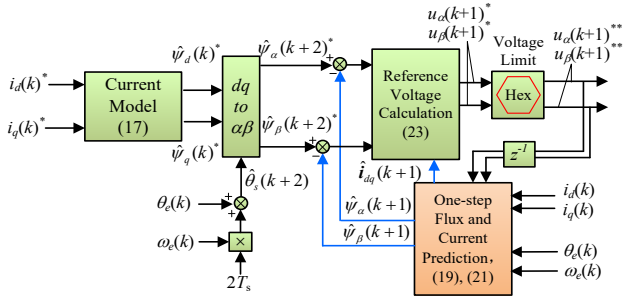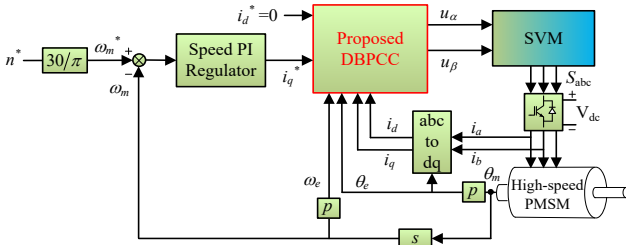

Fig. 5 Block diagram of the proposed DBPCC

Fig. 6 Block diagram of speed regulated high-speed SPMSM drive system with the proposed DBPCC

V. SIMULATION STUDIES

Extensive simulations have been performed in MATLAB/ SIMULINK to validate the effectiveness of the proposed DBPCC. The parameters of the high-speed drives are given in Table I. The inverter nonlinearity is not considered in the simulation. The switching frequency and sampling frequency are both set to 10 kHz. The resultant SFR is 10 at the rated speed of 30,000 rpm and 6 at the maximum speed of 50,000 rpm.

A. Effectiveness of proposed DBPCC

Simulations of the high-speed motor accelerating from standstill to 50,000 rpm under a constant load torque with the max reference q-axis current of 50 A have been performed to verify the effectiveness of the proposed DBPCC. As can been seen from Fig. 7, with the proposed method, the dq-axis currents can always be in good control and exactly follow the reference currents at any speed. The control problems with the conventional DBPCCs present in Fig. 4 have been effectively

addressed. It is worth noting that the increasing ripples in the torque waveform is caused by the SFR reduction as the speed rises. The dq-axis currents shown in the figure are the sampled values hence free of switching ripples.
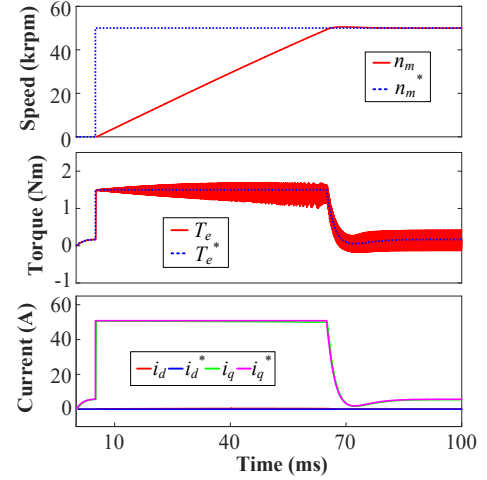

Fig. 7 Speed, torque and sampled dq-axis current waveforms of the prototype high-speed PMSM drives accelerating form standstill to 50,000 rpm using the proposed method.

Besides, by comparing the speed waveforms in Fig. 4 (b) and Fig. 7, it can be seen that the motor speed response is less affected although with the deteriorated current/torque control under the conventional DBPCC with compensation. It can be attributed to the fact that the speed ripples caused by the high torque ripples are greatly damped in high-speed drives due to its large stored kinetic energy at high speeds. Therefore, it manifests comparison of speed response cannot well indicate the fundamental problems of the conventional DBPCCs. Instead, the underpinning current control performances are focused in this paper.

B. Applicable SFR ranges of different DBPCC methods

According to the previous analysis, it is the average voltage errors described in (5) and (6) that determine the model accuracy of the conventional DBPCCs. They are reflected in the dq-axis current control error as shown in Fig. 4, which can be readily measured. However, it may be difficult to directly identify the current control error of the conventional DBPCCs in the whole high-speed region, since the high-speed drive may lose control at high speeds. Therefore, an indirect method based on two-step current prediction is proposed and used in this section, to quantitatively evaluate the model errors caused by the rotor movement in high-speed region and generally identify the applicable SFR ranges of different DBPCC methods.
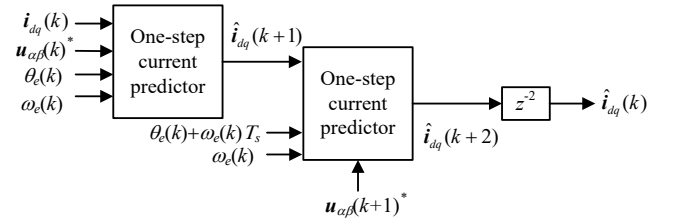

Fig. 8 The general block diagram of the constructed two-step dq-axis current predictor for different DBPCCs.

Given the intrinsic feature of two-step prediction of DBPCC, the proposed quantitative evaluation scheme is based on the

constructed two-step current predictors associated with different DBPCCs, as shown in Fig. 8. For the conventional DBPCCs, the one-step current predictor is based on (3) and (5) or (3) and (6), accordingly. For the proposed DBPCC, the one-step current predictor is based on (19) and (21). The predicted dq-axis currents are delayed by two steps and then compared with the sampled values to evaluate the model error caused by the rotor movement in different DBPCCs. Since the proposed DBPCC can give stable and good current control over the whole speed range, the constructed two-step current predictors associated with different DBPCCs are implemented simultaneously meanwhile the high-speed machine is controlled by the proposed DBPCC.

Fig. 9 plots the relative prediction errors of the two-step predictors as a function of SFR associated with different DBPCCs, when the machine speed increases from 0 to 50,000 rpm (SFR=6). The nominal current is set to 50 A. As can be seen, as the SFR decreases below a critical value, the prediction errors rise nearly exponentially with the conventional DBPCCs. It can be concluded that to have the similar accuracy to the proposed DBPCC, the SFRs with the conventional DBPCC without rotor movement compensation should be higher than 50 and that with rotor movement compensation should be larger than 20. Additionally, the rapid increase of prediction error around 10 with rotor movement compensation also provides an explanation for the phenomenon that the rotor movement compensation would lose effectiveness when the SFR is less than 10, as reported for FOC [6].
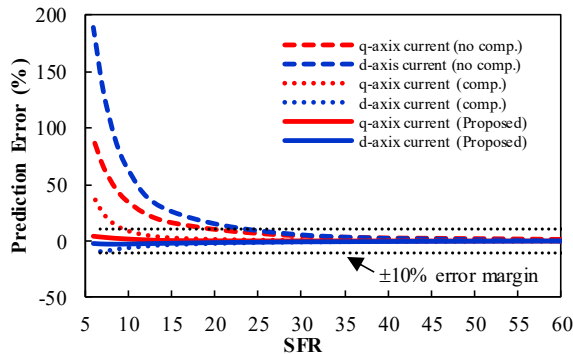

Fig. 9 Prediction errors of the constructed two-step predictors as a function of SFR, associated with different DBPCC schemes.

It should be noted that in order to investigate the worst-case scenario, the sampling frequency is set to the switching frequency in this paper. Alternatively, the sampling frequency can be increased to the twice of the switching frequency or the field programmable gate array (FPGA) based oversampling technique [27] can be employed. In these cases, the rotor movement over the control period is reduced hence the effective SFR of control will increase at a given speed. However, the same analyses, results and conclusions as above can be derived when the effective SFR reduces to a low value at high speeds.

VI. EXPERIMENT RESULTS

A. Experiment set-up

Fig. 10 shows the photos of the experiment step-up. The prototype high-speed motor, whose parameters are given in Table I, is mounted via an in-line torque transducer onto the dynamometer and enclosed in a concrete pit for the safety purpose. The control for the prototype high-speed motor drive is based on the real-time digital platform from OPAL, i.e. OP5600. The off-the-shelf three-phase IGBT power module SKiM459GD12E4 from SEMIKRON is used. As shown in Fig. 10 (c), the high-speed motor drive and high-speed dyno in the spin pit can be operated and monitored remotely in real-time.
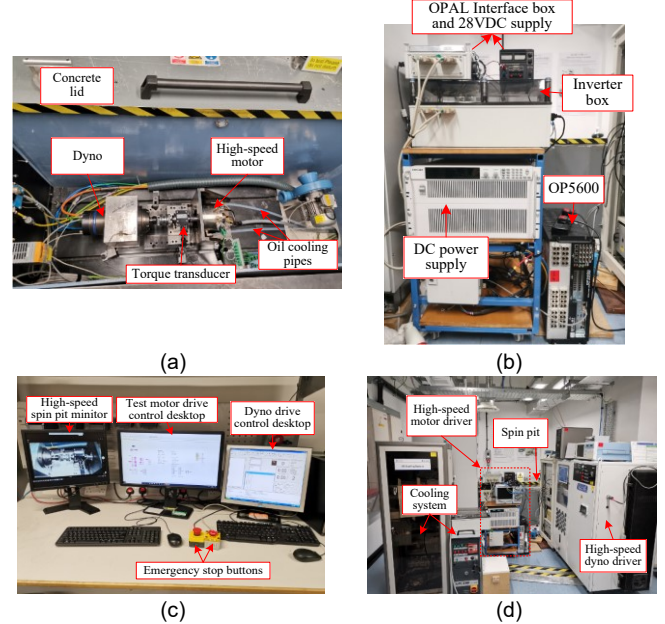

Fig. 10. Experiment set-up. (a) High-speed motor mounted in a spin pit. (b) High-speed motor driver. (c) Remote operation desk. (d) Overall view of the test rig.

B. Inverter nonlinearity compensation

As is well known for predictive control, in order to obtain good control performance, the accurate machine model should be used. Hence, the measured machine parameters in Table I are employed for all the DBPCCs in the experiments. However, the inverter nonlinearity is unavoidable and can cause significant control error at low speed, depending on the switching devices being used.
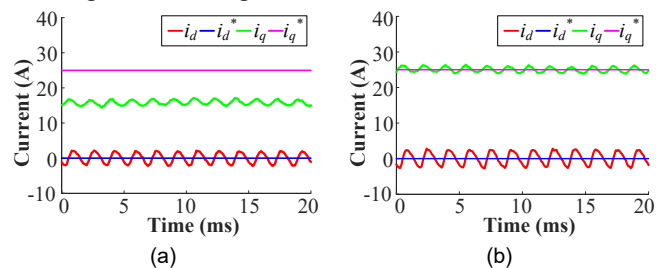

Fig. 11. dq-axis currents with the dead-time of 2 μs and q axis current reference of 25A at 3,000 rpm. (a) Without any compensation. (b) With LUT based compensation.

Fig. 11 (a) shows the sampled dq-axis currents in the steady state at 3000 rpm with the reference q-axis current of 25A under the proposed DBPCC. As can be seen, due to neglect of the inverter voltage drop and dead-time effect in the control algorithm, the q-axis current have a conspicuous offset error. The experiments with different q-axis current demands have also been performed and Fig. 12 plots the relationship between

the q-axis current demand and the average value of the measured actual q-axis current.

To compensate the average current control error caused by the inverter nonlinearity, the LUT obtained from Fig. 12 is added between the input reference and the DBPCC controller, as shown in Fig. 13. As can be seen in Fig. 11 (b), after compensation, the current control error caused by inverter nonlinearity can be effectively eliminated.
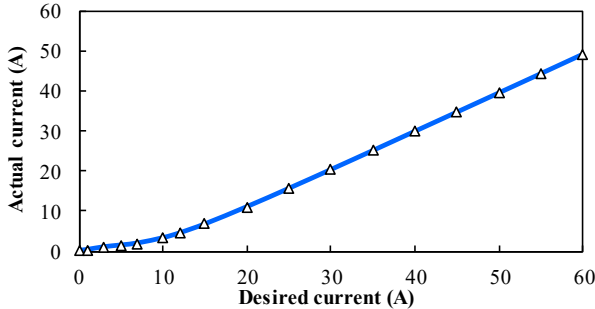

Fig. 12. Measured relationship between the desired q-axis current and the average of the actual output (without any compensation).
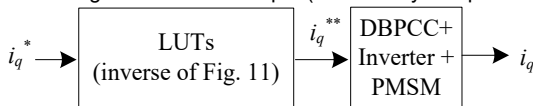

Fig. 13. Block diagram of inverter voltage drop compensation for all the DBPCC methods.

The tests have been repeated for high speeds and the conventional DBPCCs at 3,000 rpm as well. These experiment results are not shown since they are similar to those in Fig. 11, i.e. the same amounts of q-axis current error are observed without compensation while when the compensation is applied, the current control error can be effectively removed. This can be understood by the fact that the inverter voltage drop is only dependent on current and dead-time [28], and hence independent of speed and types of DBPCC. Thus, this LUT based compensation method for inverter nonlinearity is employed for all the DBPCCs in the subsequent experiments. After this compensation, the steady-state current control errors of DBPCCs are no longer affected by the inverter nonlinearity.

C. Steady-state performance

In order to investigate the influence of the machine speed on the current control accuracy with different DBPCCs, the prototype machine is operated under current control with the reference q-axis current of 25 A, while the machine speed is varied by the dynamometer. The actual machine parameters and the aforementioned inverter nonlinearity compensation method are employed.

Fig. 14 shows the experiment results with different DBPCCs when the machine is accelerated from 1,000 rpm (SFR=300) to 35,000 rpm (SFR=8.57) by the dynamometer. As can be seen, at low speeds with high SFRs, all the control methods exhibits good current control accuracy. However, as the speed rises, i.e., the SFR reduces, the current control errors with the conventional methods increases rapidly. In contrast, the proposed DBPCC control accuracy is hardly affected by the speed. Moreover, as can be seen in Fig. 14 (a) and (b), the performance of the conventional DBPCC without and with rotor movement compensation deteriorates when the speed is

higher than 6,000 rpm (SFR=50) and 15,000 rpm (SFR=20), respectively. It confirms the conclusion derived from the previous quantitative analysis, that to obtain similar control performance, the SFR for the conventional DBPCC without and with compensation should be larger than 50 and 20, respectively.
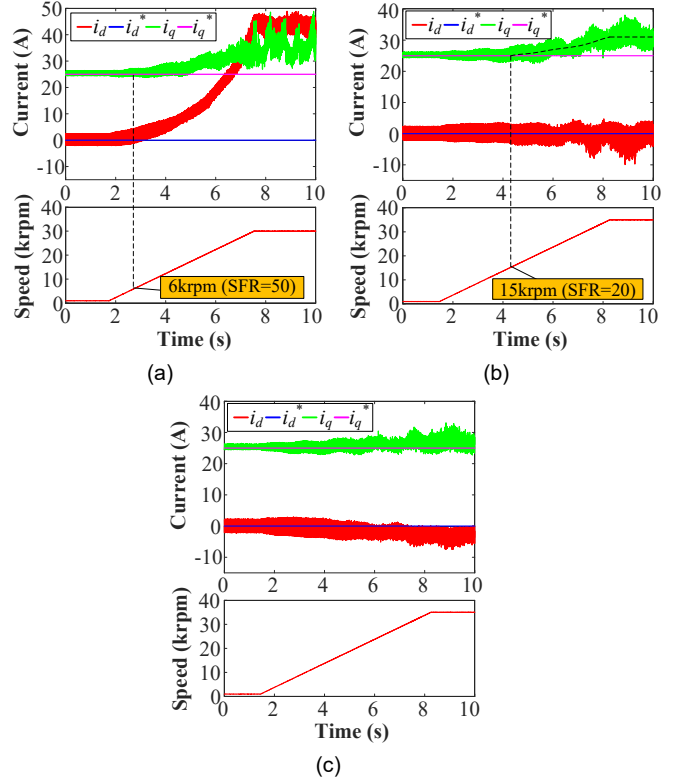

Fig. 14 dq-axis currents at various speeds. (a) Conventional DBPCC without compensation. (b) Conventional DBPCC with compensation. (c) Proposed DBPCC.

Additionally, it is evident that the conventional DBPCC with compensation is better than that without compensation in control accuracy. It infers that the rotor movement compensation, i.e. (7), should be employed for the conventional DBPCC at high speeds. Therefore, the conventional DBPCC without compensation is not considered in the following experiments unless stated otherwise.

The steady-state phase currents and their harmonic spectrum with the proposed DBPCC at the low speed of 3,000 rpm and the rated high speed of 30,000 rpm are shown in Fig. 15 (a) and (b), respectively. The total harmonic current, I_h, is defined as the root-mean-square of all the harmonics and the total current distortion (THD) is calculated from dividing the total harmonic current by the fundamental current, I_1. As can be seen, at the high speed, the switching harmonics are dominated in the phase currents and the current THD increases due to the reduction in the number of switchings per fundamental cycle, i.e. lower SFR. In addition, it can be seen that the phase currents at low speeds contain the 5th and 7th harmonics, which can be attributed to the harmonic voltage distortions caused by the inverter nonlinearity [28]. This corresponds to the conspicuous dq-axis current ripples in Fig. 11 as well. However, these harmonics and dq-axis current ripples would reduce and become insignificant at the rated high speed, as evident in the phase currents in Fig.

15 (b) at 30,000 rpm and the dq-axis current waveform shown subsequently in Fig. 18 (b).

The total harmonic current, normalized to the rated current of 50 A, at different speeds with the proposed method and the conventional DBPCC with compensation are compared in Fig. 16. As verified previously, to yield accurate dq-axis current control, the conventional DBPCC with compensation should operate with SFR>20, i.e. the speed below 15,000 rpm and thus the results of the conventional DBPCC with compensation are only shown in this speed range. As is seen, the two DBPCC methods exhibit almost identical total current distortions. It can be attributed to the fact that both the DBPCCs are based on SVM, which fundamentally determines the current harmonic distortions at high speeds.
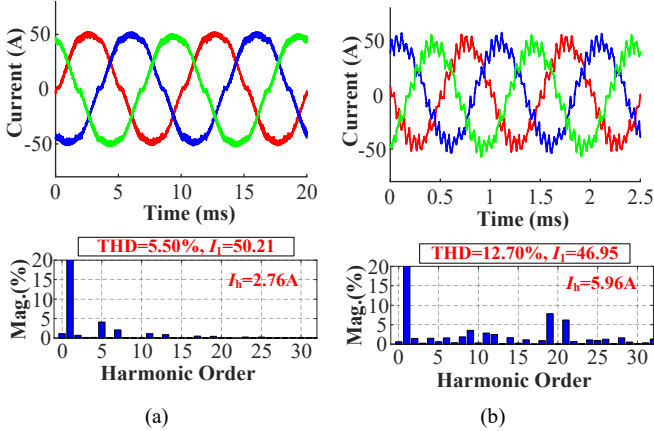

Fig. 15. Phase currents with the proposed method. (a) 3,000 rpm. (b) 30,000 rpm.
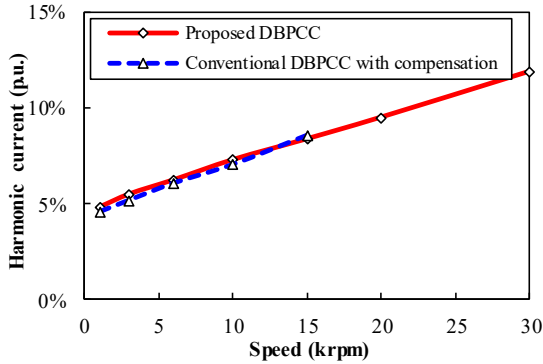

Fig. 16 Comparison of total harmonic currents with the proposed method and the conventional DBPCC with compensation.

D. Transient performances

Fig. 17 (a) and Fig. 18 (a) compare the current transient control performances under conventional DBPCC with rotor movement compensation and proposed method at 10,000 rpm. As can be seen, the control performance of conventional DBPCC is similar to the proposed method at 10,000 rpm. It is because that the switching/sampling frequency of 10 kHz leads to SFR=30, which is larger than the identified critical SFR for the conventional DBPCC with rotor movement compensation.

However, as shown in Fig. 17 (b) and Fig. 18 (b), where the current transient control experiments are repeated at a higher speed, i.e. 30,000 rpm (SFR=10), the control performance of conventional DBPCC deteriorate significantly although the rotor movement compensation has been employed. Large cross-coupling between the dq axes can be observed in the conventional DBPCC. However, as can be seen in Fig. 18 (b), the excellent deadbeat control of dq-axis currents can be still achieved with the proposed method.

Based on the transient responses at SFR=30 and SFR=10 as shown in Fig. 17, the previous identified applicable SFR range for the conventional DBPCC with rotor movement compensation, namely SFR<20, has been verified as well.
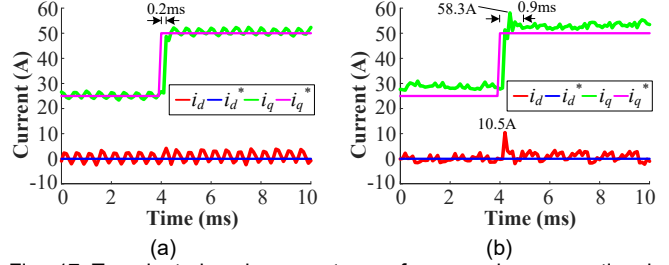

Fig. 17 Transient dq-axis current waveforms under conventional DBPCC with rotor movement compensation. (a) 10,000 rpm (SFR=30). (b) 30,000 rpm (SFR=10).
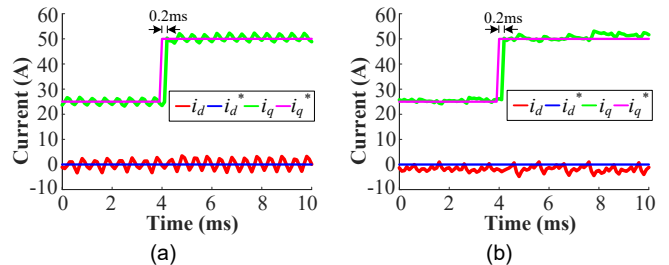

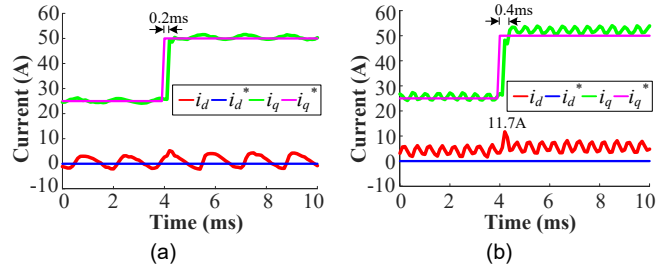Fig. 18. Transient dq-axis current waveforms under proposed DBPCC. (a) 10,000 rpm (SFR=30). (b) 30,000 rpm (SFR=10).

Fig. 19 Transient dq-axis current waveforms under conventional DBPCC without rotor movement compensation. (a) 3,000 rpm (SFR=100). (b) 10,000 rpm (SFR=30).

Similarly, to confirm the applicable range of the conventional SFR range of the conventional DBPCC without rotor movement compensation, the similar transient experiments at 3,000 rpm (SFR=100) and 10,000 rpm (SFR=30) under the conventional DBPCC without rotor movement compensation have been performed. As can be seen in Fig. 19 (a), within the identified applicable SFR range, i.e. SFR>50, the dq-axis currents can be controlled in the nearly ideal deadbeat fashion at 3,000 rpm (SFR=100) albeit with the current ripples caused by the inverter nonlinearity. However, as shown in Fig. 19 (b), at 10,000 rpm where SFR is lower than 50, the dq-axis cross-coupling in transient arises in addition to the offset current error. By comparison of Fig. 19 (b) and Fig. 17 (a), the necessity of rotor movement compensation in the conventional DBPCC to extend its applicable speed and SFR ranges is demonstrated.

To highlight the superiorities of the proposed DBPCC against the FOC, which is still dominant control technique for PMSM drives in industry, the experiments under the state-of-the-art FOC [5] with feedforward decoupling, the delay and rotor movement compensation and the actual machine parameters under the same conditions of Fig. 17 and Fig. 18 are performed. As is seen in Fig. 20, at 10,000 rpm (SFR=30), the performance of the FOC is acceptable albeit the dynamic response is slightly slower than that of the DBPCC methods. However, at the high speed of 30,000 rpm (SFR=10), large cross-coupling occurs and the current response is greatly slowed. In contrast, as shown in Fig. 18, the control performance of the proposed method is not affected by the increase of speed.
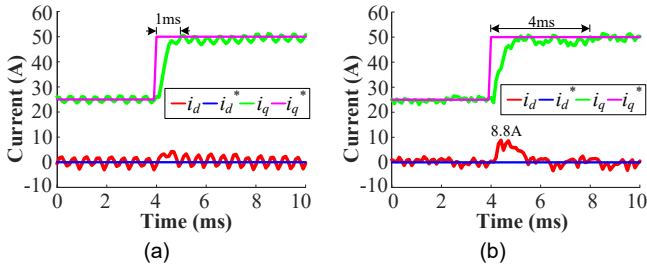

Fig. 20 Transient dq-axis current waveforms under FOC with rotor movement compensation [5]. (a) 10,000 rpm (SFR=30). (b) 30,000 rpm (SFR=10).

E. Parameter sensitivity

Extensive experiments with detuned parameters, i.e. PM flux linkage and dq-axis inductances have also been performed to test the parameter sensitivity of proposed DBPCC.

Fig. 21 shows the dq-axis current waveforms at the rated speed, i.e. 30,000 rpm, when the load current steps from 25 A to 50A. As can be seen, the parameter mismatch will introduce offset current errors in steady states. While the fast dynamic response of the control is less affected and no oscillation that could potentially affect system stability has been observed.
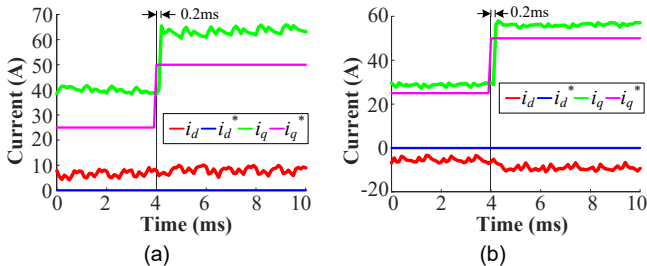

Fig. 21. dq-axis currents during q-axis current step transients at rated speed with proposed DBPCC under detuned parameters. (a) 20% over-estimation in PM flux linkage. (b) 20% over-estimation in dq axis inductances.

For the comparison purpose, the experiments using the conventional DBPCC with compensation have been carried out at the same conditions as Fig. 21. As can be seen in Fig. 22 (a), under the PM flux linkage mismatch, the dynamic performance of the conventional DBPCC is less affected while the steady-state current errors are larger than those with the proposed method in Fig. 21 (a). On the other hand, when the inductance is not accurate as shown in Fig. 22 (b), the transient performance of the conventional DBPCC is significantly

deteriorated with large dq-axis cross-coupling, overshoots and oscillations, although the magnitudes of the steady-state current error are close to those with the proposed method.
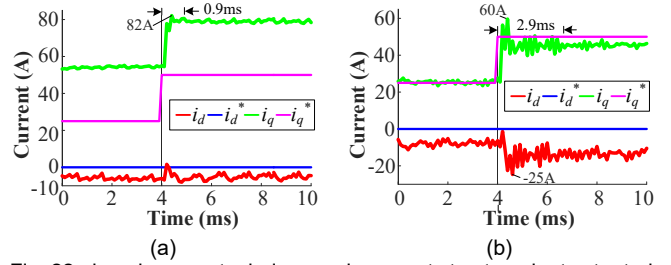

Fig. 22. dq-axis currents during q-axis current step transients at rated speed with proposed DBPCC under detuned parameters. (a) 20% over-estimation in PM flux linkage. (b) 20% over-estimation in dq axis inductances.

As can be seen, the proposed method also outperforms the conventional DBPCC under parameter mismatch, mainly with deterioration in the steady-state control accuracy. The experiments with under-estimated parameters have also been conducted and the similar observation and conclusion can be made. Besides, the experiments with the proposed method under phase resistance mismatch have also been performed, which confirm that the phase resistance mismatch is negligible at high speeds. By ways of example, the result at the rated speed under 50% under-estimation in phase resistance is shown in Fig. 23, which is similar to that in Fig. 18 (b).
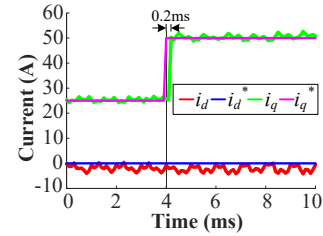

Fig. 23. dq-axis currents during q-axis current step transients at rated speed with proposed DBPCC under 50% under-estimation in phase resistance.

Additionally, in reality, the detuning of the PM flux linkage and inductance mismatches would be less than 10%, and hence the current control error will be much lower than those presented in Fig. 21. Moreover, the steady-state current error in the q-axis can be compensated by the speed controller in a speed feedback drive. However, to further improve the current control performance with proposed DBPCC, parameter uncertainty compensation schemes, such as the disturbance observer technique [15]–[17] can be a future research topic.

VII. CONCLUSIONS

This paper has presented a novel DBPCC for high-speed PMSMs drive with low SFRs. The sampling delay and rotor movement effect are accurately considered. The proposed method can realize excellent deadbeat control of dq-axis currents at high speeds even at very low SFRs. The dq-axis cross-coupling during transients at high-speeds can be virtually eliminated. Moreover, the rotor movement influence on the conventional DBPCCs with and without compensation have

been both analyzed. The applicable SFR ranges of the conventional DBPCCs have been quantitatively identified. Simulations and experiments on a high-speed PMSM drive have been performed and validated the proposed method and the analysis.

Although the proposed method is described and demonstrated by the example of high-speed SPMSM drive in this paper, it can also be applied for IPMSM drives based on a high-fidelity machine model [25].

REFERENCES

[1] W. Feng, H. Ding, S. Lee, F. Chen, T. Jahns, and B. Sarlioglu, "Design of a 100 kW Surface Permanent Magnet Machine with Wide Constant Power Speed Ratio for Traction Applications," in *2020 IEEE Transportation Electrification Conference & Expo (ITEC)*, 2020, vol. 650, pp. 456–461.

[2] S. Bozhko *et al.*, "Development of Aircraft Electric Starter–Generator System Based on Active Rectification Technology," *IEEE Trans. Transp. Electrif.*, vol. 4, no. 4, pp. 985–996, Dec. 2018.

[3] A. Balachandran, M. Boden, Z. Sun, S. J. Forrest, J. D. Ede, and G. W. Jewell, "Design, construction, and testing of an aero-engine starter-generator for the more-electric aircraft," *J. Eng.*, vol. 2019, no. 17, pp. 3474–3478, Jun. 2019.

[4] R. Abebe, M. Di Nardo, D. Gerada, G. Lo Calzo, L. Papini, and C. Gerada, "High speed drives review: Machines, converters and applications," *IECON Proc. (Industrial Electron. Conf.*, pp. 1675–1679, 2016.

[5] Bon-Ho Bae and Seung-Ki Sul, "A compensation method for time delay of full-digital synchronous frame current regulator of pwm ac drives," *IEEE Trans. Ind. Appl.*, vol. 39, no. 3, pp. 802–810, May 2003.

[6] J.-S. Yim, S.-K. Sul, B.-H. Bae, N. R. Patel, and S. Hiti, "Modified Current Control Schemes for High-Performance Permanent-Magnet AC Drives With Low Sampling to Operating Frequency Ratio," *IEEE Trans. Ind. Appl.*, vol. 45, no. 2, pp. 763–771, 2009.

[7] Hongrae Kim, M. W. Degner, J. M. Guerrero, F. Briz, and R. D. Lorenz, "Discrete-Time Current Regulator Design for AC Machine Drives," *IEEE Trans. Ind. Appl.*, vol. 46, no. 4, pp. 1425–1435, Jul. 2010.

[8] J. Holtz, J. Quan, J. Pontt, J. Rodríguez, P. Newman, and H. Miranda, "Design of fast and robust current regulators for high-power drives based on complex state variables," *IEEE Trans. Ind. Appl.*, vol. 40, no. 5, pp. 1388–1397, Sep. 2004.

[9] M. Koc, J. Wang, and T. Sun, "Stator flux oriented control for high performance interior permanent magnet synchronous machine drives," *IET Conf. Publ.*, vol. 2016, no. CP684, pp. 6 .-6 ., 2016.

[10] S. Vazquez, J. Rodriguez, M. Rivera, L. G. Franquelo, and M. Norambuena, "Model Predictive Control for Power Converters and Drives: Advances and Trends," *IEEE Trans. Ind. Electron.*, vol. 64, no. 2, pp. 935–947, Feb. 2017.

[11] J. S. Lee, C. H. Choi, J. K. Seok, and R. D. Lorenz, "Deadbeat-direct torque and flux control of interior permanent magnet synchronous machines with discrete time stator current and stator flux linkage observer," *IEEE Trans. Ind. Appl.*, vol. 47, no. 4, pp. 1749–1758, 2011.

[12] L. Springob and J. Holtz, "High-bandwidth current control for torque-ripple compensation in PM synchronous machines," *IEEE Trans. Ind. Electron.*, vol. 45, no. 5, pp. 713–721, 1998.

[13] G.-K. Hung, C.-C. Chang, and C.-L. Chen, "Analysis and implementation of a delay-compensated deadbeat current controller for solar inverters," *IEE Proc. - Circuits, Devices Syst.*, vol. 148, no. 5, p. 279, 2001.

[14] A. D. Alexandrou, N. Adamopoulos, and A. Kladas, "Development of a Constant Switching Frequency Deadbeat Predictive Control Technique for Field-Oriented Synchronous Permanent-Magnet Motor Drive," *IEEE Trans. Ind. Electron.*, vol. 63, no. 8, pp. 5167–5175, Aug. 2016.

[15] P. Mattavelli, "An Improved Deadbeat Control for UPS Using Disturbance Observers," *IEEE Trans. Ind. Electron.*, vol. 52, no. 1, pp. 206–212, Feb. 2005.

[16] X. Zhang, B. Hou, and Y. Mei, "Deadbeat Predictive Current Control of Permanent-Magnet Synchronous Motors with Stator Current and Disturbance Observer," *IEEE Trans. Power Electron.*, vol. 32, no. 5, pp. 3818–3834, May 2017.

[17] Y. Yao, Y. Huang, F. Peng, J. Dong, and H. Zhang, "An Improved Deadbeat Predictive Current Control With Online Parameter Identification for Surface-Mounted PMSMs," *IEEE Trans. Ind. Electron.*, vol. 67, no. 12, pp. 10145–10155, Dec. 2020.

[18] M. Tang, A. Gaeta, A. Formentini, K. Ohyama, P. Zanchetta, and G. Asher, "Enhanced DBCC for high-speed permanent magnet synchronous motor drives," *IET Power Electron.*, vol. 9, no. 15, pp. 2880–2890, Dec. 2016.

[19] R. S. Dastjerdi, M. A. Abbasian, H. Saghafi, and M. H. Vafaie, "Performance Improvement of Permanent-Magnet Synchronous Motor Using a New Deadbeat-Direct Current Controller," *IEEE Trans. Power Electron.*, vol. 34, no. 4, pp. 3530–3543, Apr. 2019.

[20] L. Jarzebowicz, "Errors of a Linear Current Approximation in High-Speed PMSM Drives," *IEEE Trans. Power Electron.*, vol. 32, no. 11, pp. 8254–8257, 2017.

[21] J. A. Haylock, B. C. Mecrow, A. G. Jack, and D. J. Atkinson, "Enhanced current control of high-speed PM machine drives through the use of flux controllers," *IEEE Trans. Ind. Appl.*, vol. 35, no. 5, pp. 1030–1038, 1999.

[22] X. Yuan, I. Laird, and S. Walder, "Opportunities, Challenges, and Potential Solutions in the Application of Fast-Switching SiC Power Devices and Converters," *IEEE Trans. Power Electron.*, vol. 36, no. 4, pp. 3925–3945, 2021.

[23] F. Briz, M. W. Degner, and R. D. Lorenz, "Analysis and design of current regulators using complex vectors," *IEEE Trans. Ind. Appl.*, vol. 36, no. 3, pp. 817–825, 2000.

[24] Y. Wang, S. Tobayashi, and R. D. Lorenz, "A Low-Switching-Frequency Flux Observer and Torque Model of Deadbeat-Direct Torque and Flux Control on Induction Machine Drives," *IEEE Trans. Ind. Appl.*, vol. 51, no. 3, pp. 2255–2267, 2015.

[25] X. Chen, J. Wang, B. Sen, P. Lazari, and T. Sun, "A high-fidelity and computationally efficient model for interior permanent-magnet machines considering the magnetic saturation, spatial harmonics, and iron loss effect," *IEEE Trans. Ind. Electron.*, vol. 62, no. 7, pp. 4044–4055, 2015.

[26] Y. Inoue, S. Morimoto, and M. Sanada, "Comparative study of PMSM drive systems based on current control and direct torque control in flux-weakening control region," *IEEE Trans. Ind. Appl.*, vol. 48, no. 6, pp. 2382–2389, 2012.

[27] L. Rovere, A. Formentini, and P. Zanchetta, "FPGA Implementation of a Novel Oversampling Deadbeat Controller for PMSM Drives," *IEEE Trans. Ind. Electron.*, vol. 66, no. 5, pp. 3731–3741, 2019.

[28] N. Urasaki, T. Senjyu, K. Uezato, and T. Funabashi, "Adaptive Dead-Time Compensation Strategy for Permanent Magnet Synchronous Motor Drive," *IEEE Trans. Energy Convers.*, vol. 22, no. 2, pp. 271–280, Jun. 2007.

Shangjian Dai (S'19) received the B.Eng. and M.Sc. degrees in electrical engineering from Nanjing University of Aeronautics and Astronautics, Nanjing, China, in 2013 and 2016, respectively, and the Ph.D. degree in electronic and electrical engineering from the University of Sheffield, Sheffield, U.K., in 2021.

In 2016, he was an e-drive engineer with Electrified Powertrain Engineering Department, Ford Motor China Research and Engineering Center, Nanjing, China. Since October 2020, he has been a Research Associate in Power Electronics with the University of Sheffield, Sheffield, U.K. His current research interests include high-speed motor drive and control, Silicon Carbide based power electronic converters, and high-reliability motor drives for more electric aircrafts and electric vehicles.

Jiabin Wang (SM'03) received the B.Eng. and M.Eng. degrees from the Jiangsu University of Science and Technology, Zhenjiang, China, in 1982 and 1986, respectively, and the Ph.D. degree from the University of East London, London, U.K., in 1996, all in electrical and electronic engineering.

He is currently a Professor of electrical engineering with the University of Sheffield, Sheffield, U.K., where he was a Postdoctoral Research Associate from 1996 to 1997. From 1998 to 2001, he was a Senior Lecturer with the University of East London, London. His research interests include motion control and electromechanical energy conversion to electric drives for applications in automotive, renewable energy, household appliances, and aerospace sectors.

Dr. Wang is a fellow of the IET.
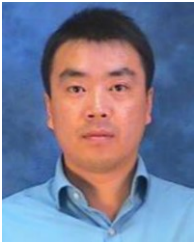
Zhigang Sun received the Ph.D. degree in electrical engineering from the University of Sheffield, Sheffield, U.K., in 2009.

He has been working in the field of electrical power systems in various professional roles in aerospace industry, semiconductor industry, and higher education since 2009. He is currently an Electrical Engineer with the Electrical Capability Group, Rolls-Royce plc, Derby, U.K.

Ellis Chong received the Ph.D. degree in electrical engineering from the University of Cambridge, Cambridge, U.K., in 2001.

He is a Chartered Electrical Engineer and has been working in the transport and power industries in the areas of electrical machines and power electronics since 2001. He is currently the Electrical Machines and Power Electronics Team Leader with the Electrical Capability Group, Rolls-Royce Plc, Derby, U.K.